Cs absorption capacity and selectivity of crystalline and amorphous Hf and Zr phosphates

Cocoro A. Nagasaka,[1] Karoly Kozma,[1] Kieran G. Brunson,[1] Chris J. Russo[2] Todd M. Alam,[3] May Nyman*[1]

[1]Department of Chemistry, Oregon State University, Corvallis, OR 97331
[2]College of Earth, Ocean and Atmospheric Sciences, Oregon State University, Corvallis, OR 97331
[3] Department of Organic Materials Science, Sandia National Laboratories, Albuquerque, NM 87185

Correspondence author: may.nyman@oregonstate.edu

Highlights

- A simplified synthesis of Zr and Hf phosphate ion exchangers is presented
- Direct comparisons of the capacity and selectivity for Cs^+ of crystalline, alpha zirconium and hafnium phosphates, and their amorphous analogues is provided
- The main factor controlling Cs-exchange capacity and selectivity is crystallinity: more amorphous analogues (either Zr or Hf) exhibit considerably better exchange behavior
- Amorphous Hf-phosphate exhibits higher selectivity and capacity for Cs^+ than the Zr-analogue, which may be attributed to the inherently poorer crystallinity of the Hf-phases

Abstract

Removal of radioactive Cs from sodium-rich solutions is a technical challenge that goes back to post World War II nuclear waste storage and treatment; and interest in this topic was reinvigorated by the Fukushima-Daiichi nuclear power plant disaster, 10 years ago. Since the 1960's there has been considerable focus on layered Zr phosphates as robust inorganic sorbents for separation of radionuclides such as Cs. Here we present synthesis and characterization, and direct comparison of Cs sorption capacity and selectivity of four related materials: 1) crystalline α-Zr phosphate and α-Hf phosphate, and 2) amorphous analogues of these. Powder X-ray diffraction, thermogravimetry, solid-state ^{31}P magic angle spinning nuclear magnetic resonance (MAS-NMR) spectroscopy, and compositional analysis (inductively coupled plasma optical emission spectroscopy and mass spectroscopy, ICP OES and ICP MS) provided formulae; respectively $M(HPO_4)_2 \cdot 1H_2O$ and $M(HPO_4)_2 \cdot 4H_2O$ (M=Hf, Zr) for crystalline and amorphous analogues. Maximum Cs loading, competitive Cs-Na selectivity and maximum Cs-Na loading followed by the above characterizations plus ^{133}Cs MAS-NMR spectroscopy revealed that amorphous analogues are considerably better Cs-sorbents (based on maximum Cs-loading and selectivity over Na) than the well-studied crystalline Zr-analogue. Additionally, crystalline α-Hf phosphate is better Cs-sorbent than crystalline α-Zr phosphate. All these studies consistently show that Hf phosphate is less crystallize than Zr phosphate, when obtained under similar or identical synthesis conditions. We attribute this to lower solubility of Hf phosphate compared to Zr phosphate, preventing 'defect healing' during the synthesis process.

Introduction

Inorganic layered metal oxides are of significant interest for many scientific applications due to their diverse and tunable compositions, and post-synthesis processability. Post-synthesis, they can be delaminated to achieve high surface area for catalysis, ion-exchanged (both cations and anions) to remove contaminants, and pillared by large ions and molecules to increase gallery space and provide function.[1] With redox-active or acidic metals, layered materials can be used for catalysis, electrochemistry, ion conduction, energy generation and storage.[2]

As ion-exchangers and sorbents, layered materials are generally endowed with high exchange capacity and rapid exchange kinetics. Post World War II legacy nuclear wastes has spurred decades of research targeting removal of radioactive Cs^+ (Cs-137) and Sr^{2+} (Sr-90) from

highly alkaline, Na-rich solutions (~ 2 molar Na) at the Hanford and Savannah River waste storage facilities.[3–7] Studied ion exchangers for nuclear waste treatment include layered oxide materials,[7] naturally occurring clays and zeolites,[8–11] zeotypes,[12–14] amorphous and semicrystalline materials,[15–19] and various other cation-exchangeable frameworks.[20–22] There has been a resurgence of interest in ion exchange materials selective for Sr^{2+} and Cs^{+} over Na^{+} during the last 10 years, since the core-meltdown of the Fukushima-Daiichi nuclear power plant followed by release of these radionuclides into the environment.[23–27]

Broadly speaking, nano-porous (zeolites and zeotypes) materials, layered materials (clays and synthetic oxides), and amorphous/semicrystalline materials all offer different advantages as ion exchangers. Layered materials, due to 2-dimensional access and expandability of the exchangeable space, exhibit rapid exchange kinetics and high exchange capacity, yet poor selectivity. Conversely, nano-porous materials may have lower exchange capacity and slower exchange rates within the 1-dimensional tunnels, yet higher selectivity based on pore size and bonding geometry within the tunnels and pores. Finally, amorphous or poorly crystalline materials have high surface area with multiple exchange sites, but they are difficult to synthesize reproducibly, and their exchange mechanisms are poorly understood.

Layered zirconium phosphate (ZrP) and hafnium phosphate (HfP) and their poorly crystalline analogues are of particular interest due to their stability in high temperatures and highly acidic conditions (as well as alkaline conditions). Structures and some ion exchange properties of amorphous and crystalline ZrP have been previously described by Clearfield[28–30], and studies of these continue to date.[31–33] Notably, the vast majority of the studies have been performed on ZrP; likely due to its cost (~60× less than Hf) and presumption that Hf is chemically identical to Zr. The crystalline forms are typified by the chemical formula, $Zr(HPO_4)_2{\cdot}1H_2O$[34,35], known as α-Zr phosphate (abbreviated α-ZrP). Briefly, in α-ZrP, Zr^{4+} is 6-coordinate with bond lengths ~2.1 Å and shares all six corners with PO_4-tetrahedra. Each PO_4 shares three corners with ZrO_6, and the fourth oxo (corner) binds a proton, pointing into the inner layer space (**figure 1**). The layers stack in the c-direction, and lattice water resides in the interlayer space. The structure of the Hf-analogue (HfP) has not been determined by single-crystal X-ray diffraction; however, Rietveld analysis of PXRD data[36] and neutron powder diffraction studies[37] describe it as isostructural, but with different ion exchange behavior. The amorphous forms are not represented in any ideal chemical formula and their exact structure is not known.

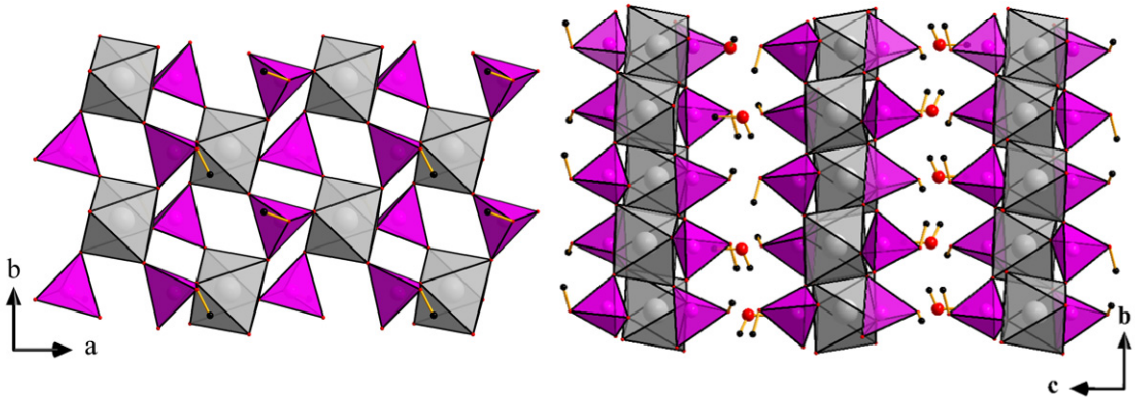

Figure 1. Two views of prior-reported α-$M(HPO_4)_2 \cdot 1H_2O$;[34,37] left is view down the *c*-axis and right is view down the *a*-axis. Zr/Hf polyhedra are silver, phosphorous polyhedra are pink. Water molecules are depicted as black (hydrogen) and red (oxygen) spheres. Hydrogen bound to the phosphates are also black.

Traditionally, the synthesis of crystalline ZrP involved a starting material of a zirconium salt, most often $ZrOCl_2 \cdot 8H_2O$, mixed into high concentrations of H_3PO_4 or lower concentrations with addition of HF as a mineralizer.[28,38–40] The HF-process is potentially dangerous and involves repeated heating and refluxing.[28,38–40] This method for synthesis is not ideal from a safety or efficiency prospective. On the other hand, the reported syntheses of amorphous ZrP does not require refluxing nor the use of HF.[33] Overall, studies of amorphous and crystalline ZrP are relatively abundant, while studies of amorphous and crystalline HfP are far scarcer.[28–30,33–41]

Ion exchange studies have been most commonly conducted using crystalline ZrP with alkalis, primarily Cs, assessing their utility in nuclear waste treatment.[41–43] Many of the results indicate Cs ion exchange efficacy for crystalline ZrP. Despite all these studies, there are few that provide side-by-side comparison and analysis of crystalline and amorphous Zr and Hf layered phosphates, or comparison between Zr and Hf analogues, and this was one of the main motivations for this study.

Here we present a simplified synthesis of crystalline ZrP and HfP, in addition to a comparative characterization and ion exchange study of both crystalline and amorphous ZrP and HfP. Characterizations included ^{31}P and ^{133}Cs solid-state MAS NMR (magic-angle spinning nuclear magnetic resonance), thermogravimetry, X-ray powder diffraction (PXRD), and compositional analyses of ion exchange solids and solutions (via ICP OES and ICP MS, inductively coupled plasma - optical emission spectrometry/mass spectroscopy). We correlate

higher selectivity and capacity for Cs with poorer crystallinity, amongst the family of compounds. For material obtained under identical synthesis conditions, amorphous HfP shows higher selectivity and capacity for Cs^+ in the presence of Na^+ than amorphous ZrP. The crystalline analogues, although with far poorer Cs-sorption performance, also show this same trend, with better performance for the Hf-analogue. PXRD of both amorphous and crystalline materials suggests that HfP phases exhibit inherently higher disorder than the ZrP phases, and we attribute this to poorer solubility of the Hf-phosphates in water, meaning 'annealing processes' are not so effective during the hydrothermal treatment. Therefore, we correlate the better Cs-sorption performance of the HfP analogues to their poorer crystallinity, defining a clear path to further optimization of these robust ion-exchange materials.

Experimental

Synthesis of amorphous ZrP and HfP. Amorphous ZrP was synthesized with $ZrOCl_2 \cdot 8H_2O$ (0.123 g) as the starting material. Teflon liners to Parr hydrothermal (23 ml) reactors were charged with the starting material plus DI-H_2O (10 mL). Under continuous stirring, H_3PO_4 (aq., 170 μL, 14.7 M) was added into the mixture. The final ratio is 6.5:1 P:Zr. The Teflon reactors were sealed in the stainless steel Parr vessels and placed into an oven at 120°C for 24 hours. After cooling, the contents of the Teflon containers were poured into a centrifuge tube for washing and separation of the solids. The white gel-like samples were rinsed with DI-H_2O and were subsequently centrifuged. This cycle of washing and centrifuging was conducted at least three times. Following washing and separation, the product was dried *in vacuo* until no water or moisture was observed. Amorphous HfP was prepared using the same method as amorphous zirconium phosphate, except the starting material was $HfOCl_2 \cdot 8H_2O$ (0.156 g).

Synthesis of crystalline ZrP and HfP. Crystalline ZrP was synthesized with $ZrOCl_2 \cdot 8H_2O$ (1.23 g) as the starting material. Teflon liners to Parr hydrothermal (23 ml) reactors were charged with the starting material plus DI-H_2O (10 mL). Under continuous stirring, H_3PO_4 (aq., 1.7 mL, 14.7 M) was added into the mixture. The final ratio is 6.5:1 P:Zr. The Teflon reactors were sealed in the stainless steel Parr vessels and placed into an oven at 220°C for 24 hours. After cooling, the contents of the Teflon containers were poured into a centrifuge tube for washing and separation of the solids. The white powders were rinsed with DI-H_2O and were subsequently centrifuged. This cycle of washing and centrifuging was conducted at least three times. Following

washing and separation, the product was dried *in vacuo* until no water or moisture was observed. Crystalline HfP was prepared using the same method as crystalline ZrP, except the starting material was $HfOCl_2 \bullet 8H_2O$ (1.56 g). This also gave a final ratio of 6.5:1 P:Hf.

Powder X-ray diffraction (PXRD). PXRD analysis was conducted on a Rigaku Miniflex with a Cu source for Kα radiation (λ = 1.5406 Å). Measurements were collected from 2θ = 2° - 60° with a step size of 1.5°/s. Samples were first ground to a fine powder with a mortar and pestle and pressed firmly and flat with a microscopic glass slide into a sample holder.

Scanning electron microscopy - energy-dispersive X-ray spectroscopy (SEM-EDX). SEM-EDX was conducted on a FEI Quanta 600F for imaging and estimating elemental compositions. Samples were mounted on a double sided conductive carbon adhesive tape atop a clean SEM sample holder. The samples were coated with gold on a Cressington 108SE sputter coater to improve conductivity and reduce charging.

Thermogravimetry (TGA) TGA data were obtained from a TA Instruments SDT Q600 scans with air as a carrier gas (100 mL min^{-1}). The samples (~15 mg each) were heated from room temperature to 800 °C at a heating rate of 10 °C min^{-1}.

MAS-NMR The solid state ^{31}P and ^{133}Cs magic angle spinning (MAS) NMR spectra were obtained on a Bruker Avance II instrument operating at 243.0 MHz and 78.7159 MHz, respectively. A 4 mm broadband MAS probe was used, with a spinning speed of 10 kHz at room temperature. The 1D direct polarization (DP) ^{31}P MAS spectra were obtained using a single pulse Bloch decay with high power TPPM ^{1}H decoupling, using a 240s recycle delay and 32 scan averaging. The ^{1}H-^{31}P cross polarization (CP) MAS NMR spectra were obtained ramped contact CP pulse with a 1 ms contact time. The 1D DP ^{133}Cs MAS NMR spectra were obtained using a 1 s recycle delay with 256 scan averages. The ^{31}P and ^{133}Cs chemical shift was references to the external standard phosphoric acid $\delta(^{31}P)$ = 0.0 ppm and 1M CsCl $\delta(^{133}Cs)$ = 0.0 ppm.

Ion exchange Three studies were performed with the four studied materials: a competitive sorption study between Cs and Na matrix, a maximum Cs-Na loading study, and a maximum Cs loading study. Crystalline or amorphous ZrP and HfP (20-50 mg) were used for each study. For maximum Cs loading, CsCl (5 mL, 0.5 M) was used. For the maximum Cs-Na loading studies, CsCl (2.5 mL, 1.0 M) was combined with NaCl (2.5 mL, 1.0 M). For the competitive sorption study between Cs and Na matrix, the ZrP and HfP samples were exposed to a matrix solution (50 mL) composed of CsCl (0.5 M) and NaCl (0.6 M). We sampled the Cs concentration remaining

before and after contact with the solutions using inductively coupled plasma optical emission spectroscopy (ICP-MS). Ion exchanged samples containing high concentrations of Na^+ ions were diluted 20-fold to reduce matrix effects and plasma loading prior to the analysis of Cs by ICP-MS. The calibration curve for Cs is shown in **figure S1**.

Compositional analysis of ZrP/HfP materials and ion exchange solutions. Solid samples were isolated from exchange solutions by centrifuging and washing with water to remove any excess surface-adsorbed alkali. They were then digested in a minimal amount of HF (5%, 1 mL) and diluted for analysis with HNO_3 (2%, 25 mL). ICP-OES and ICP-MS was conducted on a Spectros Arcos II ICP-OES for elemental analysis of P, Hf, and Zr and on a Thermoscientific iCAP RQ ICP-MS for elemental analysis of Cs and Na. Prior to analysis, all samples were further diluted with 2% HNO_3 (5-fold for ICP-OES and 125 to 5000-fold for ICP-MS)..

Results and Discussion

The syntheses presented here are very simple, without use of HF and refluxing. We believe hydrothermal processing instead of refluxing can improve reproducibility and also simplifies the apparatus. The only difference between the protocol for obtaining amorphous vs. crystalline product is the temperature, respectively 120 °C and 220 °C. PXRD analysis confirmed identify of crystallized α-Zr/Hf phosphate[34,37] for the crystalline samples (**figure 2**). A similar approach was reported recently for Zr analogues.[33] The broad diffraction peaks of the amorphous analogues do not align with the diffraction peaks of the α-Zr/Hf phosphate, meaning they are not simply smaller particles of the crystalline phases. They are similar to each other, and notably the ZrP phase has a broad peak below 10° 2θ, suggesting an interlayer spacing; and this will be discussed later. This peak is not so evident in the HfP phase, but other broad peak positions are similar between the Zr and Hf analogues. Compositional analysis by ICP-OES unambiguously showed the 2:1 P:M (M = Hf, Zr) in both the crystalline and amorphous phases (ranging from 2.002 – 2.046, P:M). The compositions are summarized in **Table 1**, along with those for the ion-exchanged samples that will be discussed throughout the text. Since the materials are synthesized hydrothermally with a ~6:1 P:M ratio, this unalterable ratio of 2:1, even for the amorphous materials, is likely a reflection on the poor solubility of Zr/Hf-HPO_4 ion pairs in the applied synthesis conditions. SEM images (**figure 3**) show thin plates and sheets on the scale of micrometers and nanometers for the

crystalline analogues. On the other hand, the amorphous ZrP and HfP show no such features at this scale; and they have almost a glassy appearance.

Table 1.
Summary of composition of acid forms and ion exchanged forms of ZrP and HfP (amorphous and crystalline)

Material	**Acid form**[1]	**Maximum Cs-loading**[2]	**Cs-Na competition**[2]
Amorphous ZrP	$Zr(HPO_4)_2•4H_2O$	$Cs_{0.48}Zr(H_{0.76}PO_4)_2•xH_2O$	$Cs_{0.55}Na_{0.019}Zr(H_{0.715}PO_4)_2•xH_2O$
Amorphous HfP	$Hf(HPO_4)_2•4H_2O$	$Cs_{0.46}Hf(H_{0.77}PO_4)_2•xH_2O$	$Cs_{1.50}Na_{0.050}Hf(H_{0.225}PO_4)_2•xH_2O$
Crystalline ZrP	$Zr(HPO_4)_2•1H_2O$	$Cs_{0.033}Zr(H_{0.98}PO_4)_2•xH_2O$	$Cs_{0.018}Na_{0.0023}Zr(H_{0.99}PO_4)_2•xH_2O$
Crystalline HfP	$Hf(HPO_4)_2•1H_2O$	$Cs_{0.037}Hf(H_{0.98}PO_4)_2•xH_2O$	$Cs_{0.024}Na_{0.150}Hf(H_{0.913}PO_4)_2•xH_2O$

[1]*based on ICP OES, ICP MS and TGA*
[2]*based in ICP OES and ICP MS, water content not determined*

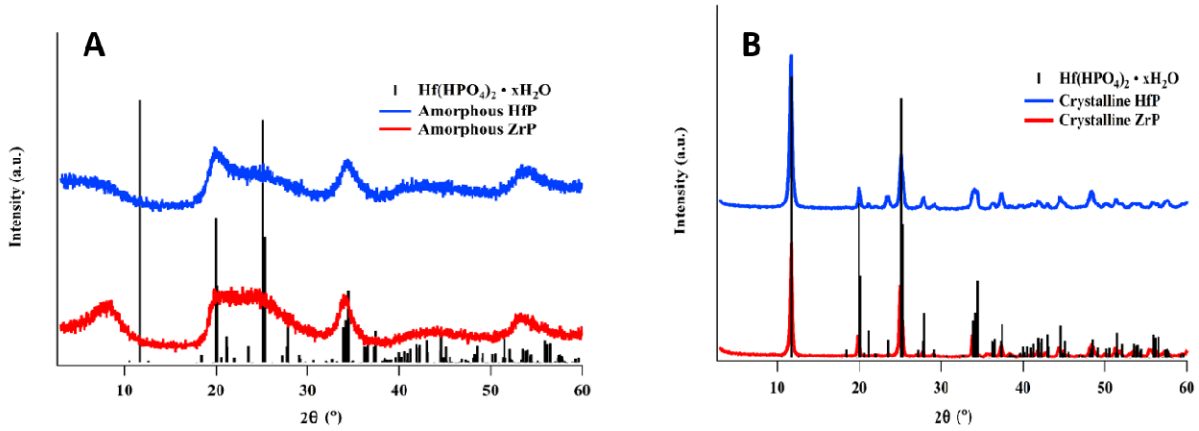

Figure 2. PXRD of amorphous (**A**) and crystalline (**B**) ZrP and HfP. Also shown is the simulated peak positions for α-$Hf(HPO_4)_2•1H_2O$.[34,37]

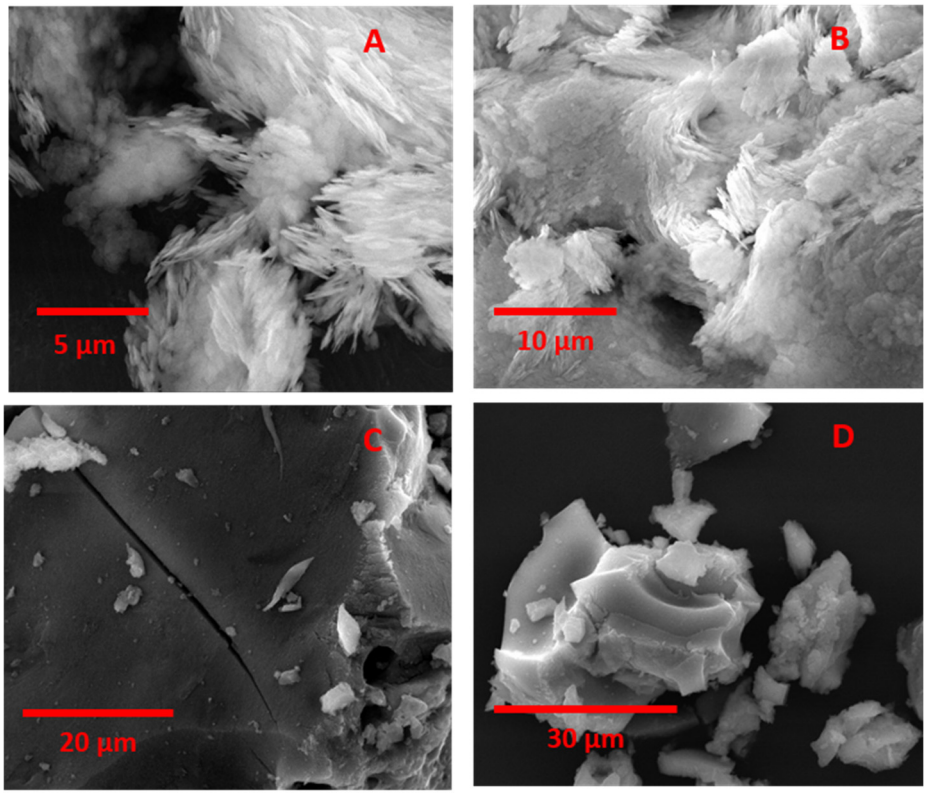

Figure 3. SEM images of (A) crystalline ZrP, (B) crystalline HfP, (C) amorphous ZrP, and (D) amorphous HfP

Thermogravimetric analysis (TGA) for all four samples are compiled in **figure 4**. Crystalline ZrP and HfP show two distinct weight loss events, respectively below 200 °C and between 400 – 600 °C. On the other hand, the amorphous analogues exhibit less distinctive weight loss curves from room temperature to approximately 800 °C. The thermal decomposition of the crystalline phases, can be described as:

$$M(HPO_4)_2 \bullet xH_2O \rightarrow M(P_2O_7) + (x+1)H_2O \qquad (1)$$

The 12% weight loss for crystalline ZrP corresponds with exactly 2 water molecules, meaning x=1, with a formula of $Zr(HPO_4)_2 \bullet 1H_2O$. This is exactly consistent with the prior reported α-ZrP.[28] Alternatively, we could describe the formula as $Zr(PO_4)_2 \bullet 2H_3O$, especially given the well-known ion-exchange behavior of the compound; and MAS NMR provides a more informed analysis (discussed later). The crystalline HfP has 10% weight loss, also consistent with a formula of $Hf(HPO_4)_2 \bullet 1H_2O$ or $Hf(PO_4)_2 \bullet 2H_3O$. The amorphous analogues do not exhibit the second high

temperature distinct weight loss event, and the total volatile content removed by heating to 800 °C is 14 wt % and 17 wt % respectively for amorphous HfP and amorphous ZrP. Amorphous Zr and Hf analogues both have ~four water molecules per formula unit based on TGA. In sum, the TGA and ICP-OES analyses together provide formulae for the amorphous materials of $Hf(HPO_4)_2 \bullet 4H_2O$ and $Zr(HPO_4)_2 \bullet 4H_2O$.

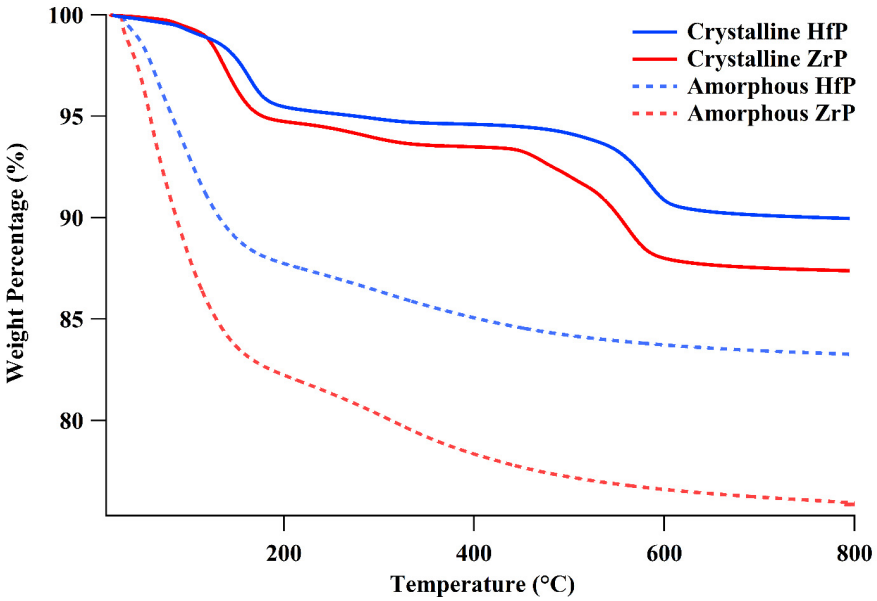

Figure 4. Thermogravimetric analysis for the crystalline HfP and ZrP, and amorphous HfP and ZrP.

^{31}P NMR. **^{31}P NMR**. The ^{31}P direct polarization (DP) MAS NMR spectra for the crystalline ZrP and HfP is shown in **figure 5a** and revealing a dominant peak at δ = 18.9 ppm (ZrP) and δ ~ -13.0 ppm (HfP). The +6 ppm higher frequency shift (more positive δ) of HfP is consistent with previous studies of different types of Zr and Hf phosphate. For example, the ~ +6 ppm high frequency shift with Hf substitution in $CsZr_2F_6PO_4 \cdot 4H_2O$ (δ = -15.7 ppm) and $CsHf_2F_6PO_4 \cdot 4H_2O$ (δ = -10.0 ppm)[44], the +7 ppm high frequency shift with Hf substitution in the $P(OHf)_4$ (δ = -16.89 ppm) and $P(OZr)_4$ (δ -24.04 ppm) environment in NASICON materials.[45] These shifts result from the polarizability of the metal cation and changes in the P-O bond strength.[46,47] In the $P(OM)_4$ (M=Zr, Hf) series, the difference between the Hf and Zr species has also been attributed to the role of f-electrons in shielding of the phosphorous nuclei.[45]

The ^{31}P MAS NMR spectra also offer some insight about the location of the protons in the crystalline ZrP and HfP. Crystalline ZrP has a single ^{31}P peak at -18.9 ppm (FWHM=166 Hz, see **figure 5a** and **Table S1**) that is also observed in the CPMAS NMR experiment. However, the peak observed by CP is ~12× weaker and most likely reflects non-optimized CP MAS conditions. The peak position is fully consistent with prior reports[48] and reflects that a single P environment is present in this material and corresponds to a P connected to 3 Zr metal centers through a bridging oxygen (corresponding to a Q^3 nomenclature).[48] The crystalline HfP analogue is different. There are four resonances observed in the ^{31}P DP MAS NMR spectrum. Three are very minor, accounting for ~5% total of the integrated peak area (**Table S1**). The two nearly overlapping peaks (-13.0 and -13.2 ppm, respectively 126 Hz and 465 Hz peakwidth) are present in ~1:1 ratio (**figure 5, Table S1**) and still correspond to Q^3 P environments. Interestingly, only the former narrower peak (δ = -13.0 ppm) is observed in the ^{1}H-^{31}P CPMAS NMR experiment. This suggests the peak at -13.2 ppm corresponds to a P environment with a very weak ^{1}H-^{31}P dipolar coupling, perhaps due to rapid exchange with water.[49] Deprotonation of this phosphorous would be expected to have a significant impact (~ 10 ppm shift) on the chemical shift, as seen in deprotonated ZrP materials and therefore is not a consistent argument.[50] The small difference in the chemical shift between these two P environments may reflect subtle variations in the hydration and the extent of hydrogen bonding for the -13.2 ppm environment.[51] Nonetheless, there are two chemically distinct P-sites in crystalline HfP, and there is only one in the analogous crystalline ZrP.

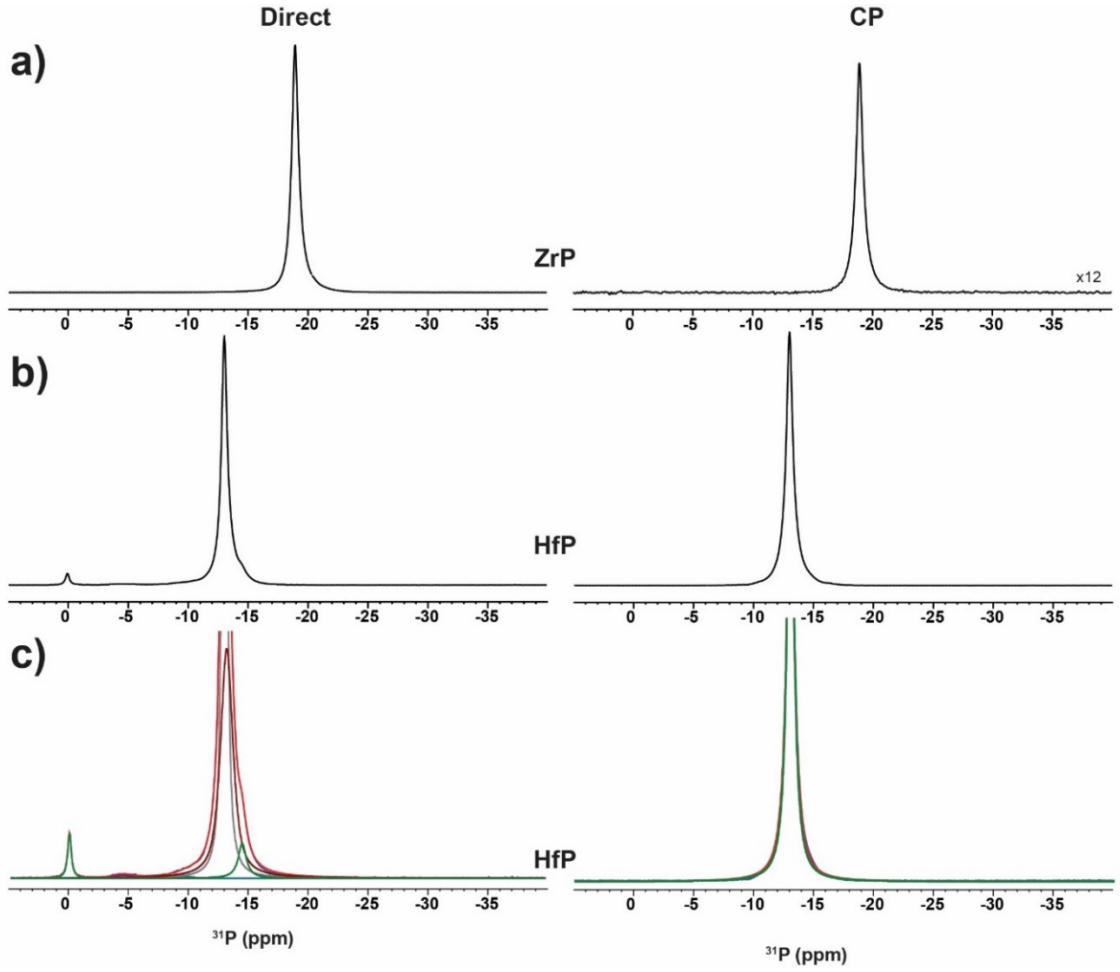

Figure 5. ^{31}P MAS NMR of crystalline ZrP and HfP. The left side of a, b and c is the direct polarization (DP) ^{31}P spectra, and the right side is the ^{1}H-^{31}P cross-polarization (CP) ^{31}P spectra. a) crystalline ZrP, b) crystalline HfP, and c) crystalline HfP showing the integration of peaks. (see also **Table S1**).

In contrast, the amorphous ZrP and HfP both have five peaks (**figure 6, Table S1**) revealing multiple unique P environments, and are consistent with micro-crystalline-type phases with different number of P-O-Zr linkages. Again the change in the chemical shift between the Hf and Zr species can be related to polarizability of the metal center and changes in the P-O bond strength.[46,47] These P environments in the amorphous materials are generally represented by broader peaks than those observed in the crystalline ZrP and HfP materials (**Figure 5**) and reflect the additional disorder present in the range of Q^n connectivity. (**figure 6**, 'n' refers to number of PO_4 corners shared by Zr/Hf). Based on prior studies of a Nafion-ZrP (poorly crystalline) membrane, the peaks can be assigned as Q^1, Q^2, Q^3 and Q^4 P environments;[52] respectively,

phosphate bridging to one, two, three and four Zr/Hf, where the Q^3 P environment dominates. Notably, the Q^3 environment is also that which is observed in the crystalline phase. The ^1H-^{31}P CPMAS NMR spectra also reveal multiple Q^n environments, but the resonances are even more broadened (**Table S1**), and a lower relative signal intensity with respect to the DP NMR spectra). These can be assigned to extremely disordered amorphous ZrP and HfP domains. The reduction in CPMAS signal intensity arises from a reduced ^1H-^{31}P dipolar interaction either due to lack of nearby protons or increased rotational dynamics, most notably for the Q^1 P species.

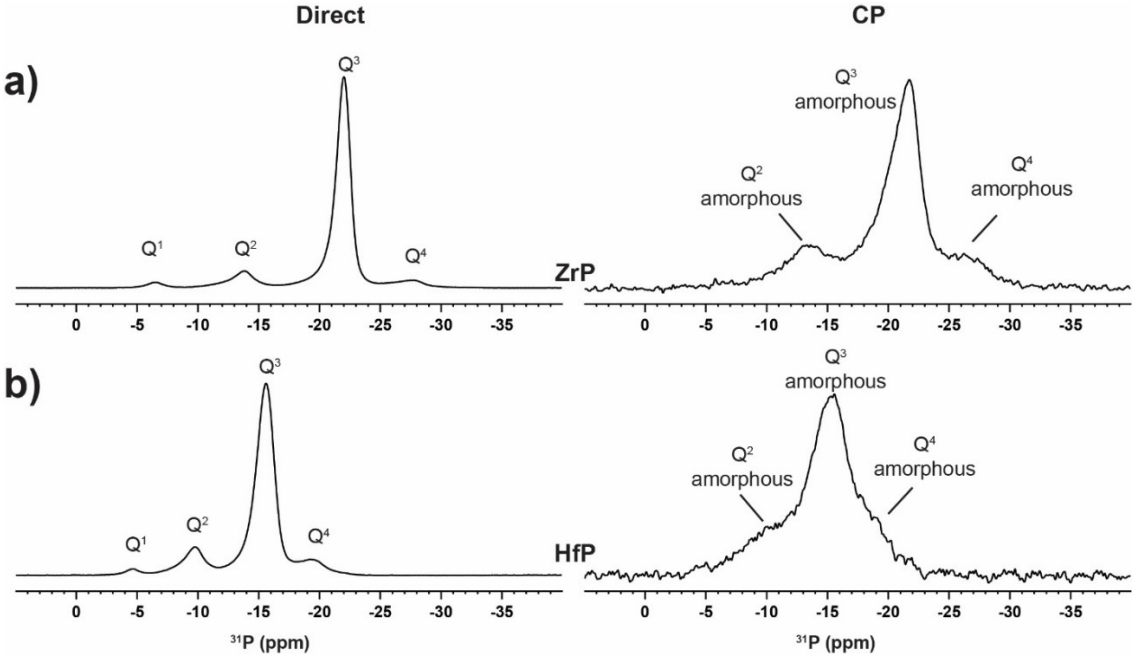

Figure 6. ^{31}P MAS NMR of amorphous ZrP and HfP. The left side of a and b is the direct polarization (DP) ^{31}P spectra, and the right side is the ^1H-^{31}P cross-polarization (CP) spectra. a) amorphous ZrP, b) amorphous HfP,

Ion exchange

In order to compare the performance of the four analogous Zr/Hf crystalline/amorphous materials for Cs removal from seawater, ion exchange studies must be performed in close to neutral conditions. Prior Cs-exchange of crystalline ZrP were carried out in CsOH media, and complete exchange was achieved.[53] Highly alkaline ion-exchange media has the obvious benefit of neutralizing the exchangeable H^+-ions, which is the driving force intercalation of alkali cations. While ion exchange studies in alkaline media are relevant to Hanford and Savannah River tank

wastes, they are not as relevant to decontamination of seawater and the current problem at Fukushima. A very recent study of Cs-sorption onto zirconium phosphate from seawater revealed relatively low selectivity, but exchange capacity was not studied.[54] On the other hand, Isao and co-workers[55] demonstrated complete K^+-exchange in the self-buffering conditions of crystalline α-HfP employing KCl solutions for exchange.

Maximum Cs-loading studies revealed the amorphous materials absorb >10× more Cs than their crystalline analogues (see **Table 1**). Compositions of crystalline Cs exchanged samples, considering the acid-form formulae determined above by ^{31}P MAS NMR and TGA are $Cs_{0.033}Zr(H_{0.98}PO_4)_2 \bullet xH_2O$ and $Cs_{0.037}Hf(H_{0.98}PO_4)_2 \bullet xH_2O$, or about 1.5% exchanged. The approximate formulae for the amorphous analogues are $Cs_{0.48}Zr(H_{0.77}PO_4)_2 \bullet xH_2O$ and $Cs_{0.46}Hf(H_{0.76}PO_4)_2 \bullet xH_2O$, or about 25% exchanged. The crystalline Hf-analogue absorbed slightly more than crystalline Zr analogue, while the amorphous Zr analogue absorbed slighted more than the amorphous Hf analogue, but they are unremarkably similar. The ^{133}Cs NMR (**Figure 7** and **Table S2)** of the exchanged phases qualitatively agree with the compositional analyses—considerably more Cs is observed in the amorphous phases than the crystalline phases, based on signal:noise ratio. For the amorphous materials, the sole ^{133}Cs resonance occurs between δ = +4 and +5 ppm, and can be assigned to a very hydrated Cs environment, based both on chemical shift and relative peak width. These peaks are up to 10× more narrow than the peaks of the crystalline samples, suggesting motion. While not studied, a dynamic Cs^+ is more likely to be back-exchanged than the static sites of crystalline ZrP and HfP. This indicates reusability of these amorphous sorbents, and should be studied in the future. A very deshielded Cs-environment is observed for the crystalline ZrP (δ ~ +50 ppm) and a very shielded Cs-environment is observed for crystalline HfP at δ = -20 ppm, as well as a minor deshielded Cs-environment at δ = -10 ppm. These respective shielding (Zr) and deshielding (Hf) values are consistent with the Cs being strongly associated within the phosphate framework, and not present as a hydrated species. The reason between the opposite shielding behavior for the Hf and Zr materials may be related to differences in the surface interactions, but the exact mechanism for the shielding variations has not been determined.

Despite the incomplete Cs-exchange, ^{31}P NMR peaks are considerable broader and greater in number for the Cs-exchanged materials (**figure S1 and Table S3**), even for the crystalline materials with very low Cs-capacity in the applied conditions. Since these phases are very insoluble, this is not related to any dissolution-precipitation reactions. We can only conclude that

disorder is induced not only by ion-exchange, but variable amounts of water in the interlayer space, migration of exchangeable protons to edge and surface sites, and so on. PXRD of the amorphous Cs-exchanged ZrP and HfP (**figure S2**) also show small changes that indicate decreased order. Specifically, for the amorphous, Cs-loaded ZrP, the broad peak below 10° 2-theta is no longer apparent.

For the ^{31}P CPMAS NMR experiments, mainly one hydrated P-environment is observed (**figure S3, Table S3**) for the crystalline samples, suggesting that the multiple environments observed in the direct spectra do not contain significant association with H^+. This observation is consistent with the argument for migration of exchangeable protons located originally on the phosphates and as H_3O^+ in the interlayer spaces to surface and edge sites. In correlation with this, simply placing any of the studied phases in water decreases the pH to around 2-4, depending on the solid:water ratio. Similarly, for the amorphous Cs-exchange materials, the CPMAS has reduced signal intensity, and highlights environments with larger line widths than observed in the direct spectra. The diminished intensity of the CP ^{1}H - ^{31}P MAS NMR peaks is much greater for the amorphous materials than the crystalline materials (**figure S3**), and this is consistent with the 10× greater $H^+ \leftrightarrow Cs^+$ exchange for the amorphous materials.

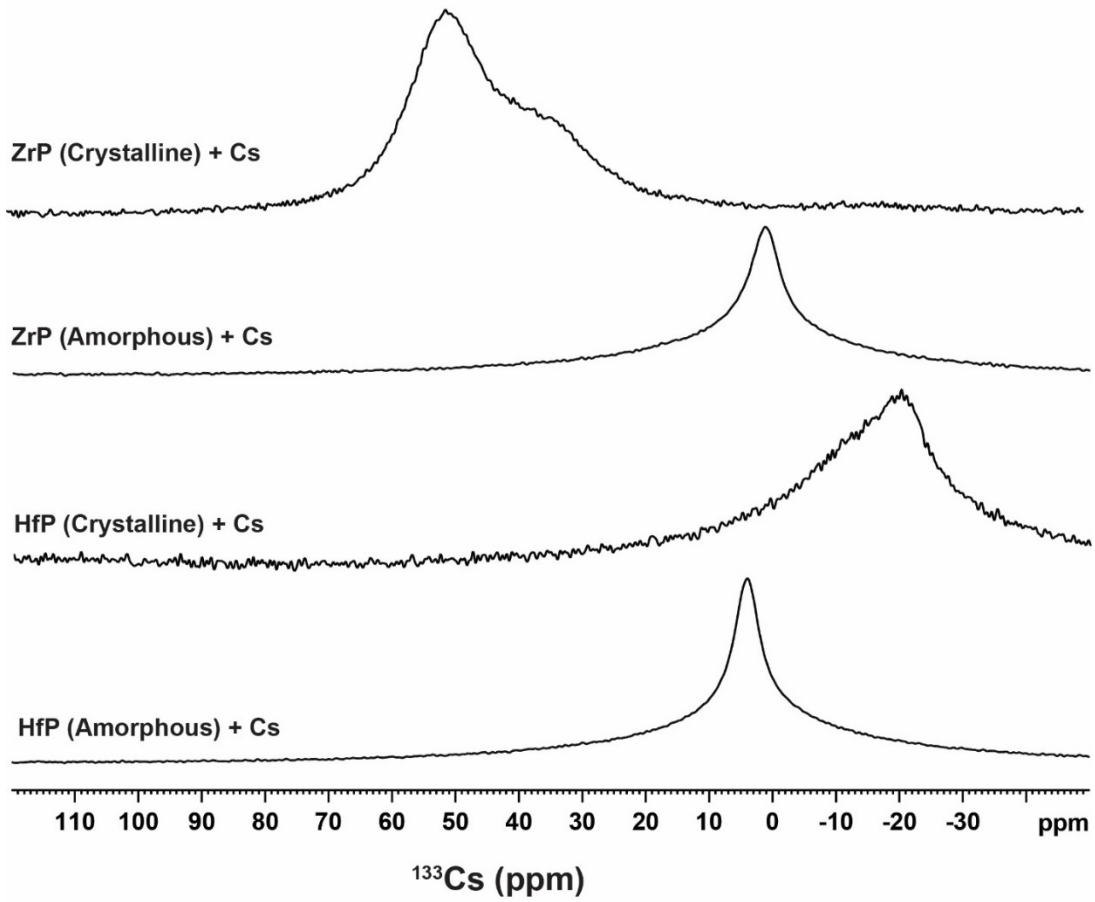

Figure 7. ^{133}Cs NMR spectra (direct polarization) of Cs-exchanged (maximum loading from CsCl solutions) amorphous and crystalline ZrP and HfP.

Competitive sorption studies (Cs^+ vs. Na^+) in 0.5 M NaCl (Na-concentration similar to that in seawater) revealed much higher selectivity for Cs by the amorphous materials compared to the crystalline materials **(figure 8)**, consistent with the trend for maximum Cs-loading. Rather than using Cs-concentrations similar to that found in ^{137}Cs-contaminated seawater, we employed a 1:1 ratio of Cs:Na, in interest of accurately measuring Cs-concentration after contact with the sorbent via ICP-MS. The concentration of Cs in a typical contaminated water sample is so low it can only be measured accurately by its radioactivity.

Amorphous HfP absorbed a maximum of ~400 ppm Cs^+ over the course of the experiment, while crystalline ZrP absorbed ~200 ppm Cs^+. On the other hand, the crystalline samples did not exhibit discernable Cs absorption, consistent with the maximum Cs-loading studies.

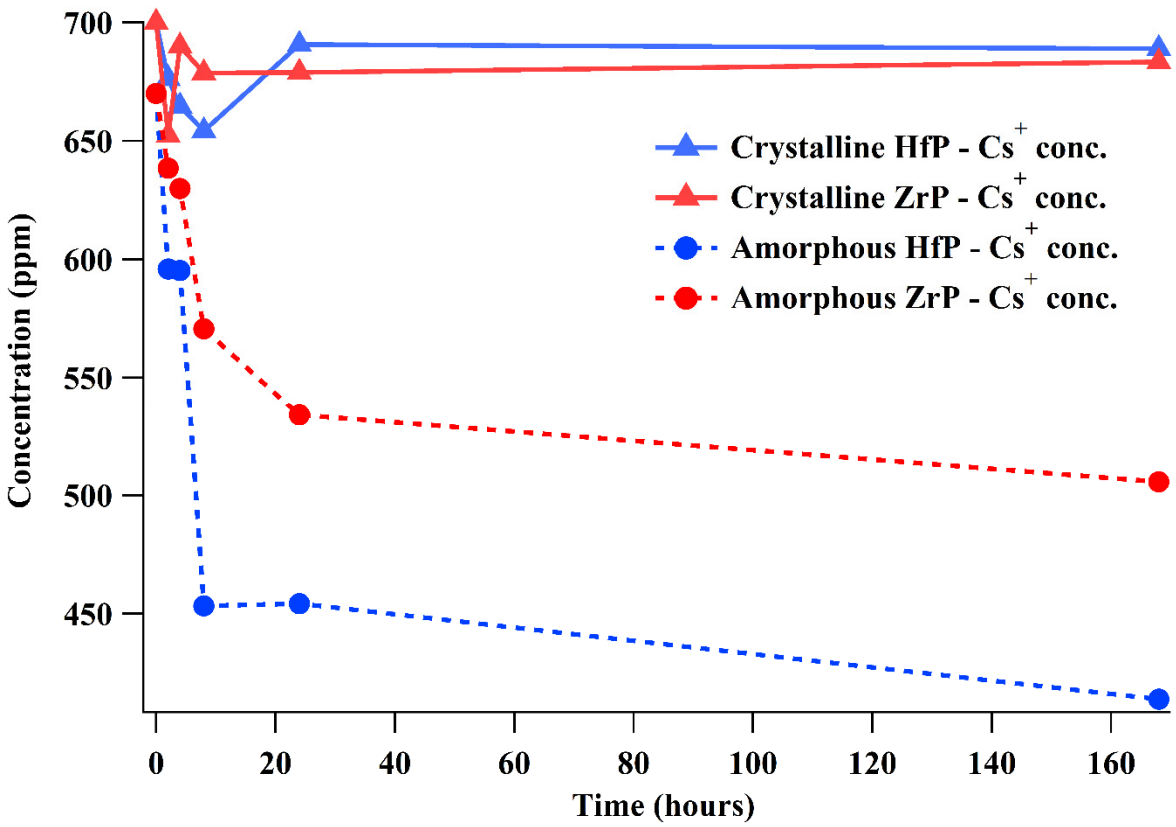

Figure 8. Plot of [Cs^+] remaining in solution from a 0.5 M Cs, 0.6 M Na solution, after contact with the amorphous and crystalline ZrP and HfP materials.

PXRD and compositional analysis of the Cs/Na exchanged samples from the competitive sorption studies

While the Cs maximum loading studies presented fairly straightforward results of higher absorption (>10×) onto the amorphous materials, and similar absorption between the Zr and Hf analogues, the results were not so straightforward for the competitive Na/Cs sorption studies (**Table 1**). The amorphous Hf-analogue absorbed 3× more Cs than the amorphous Zr analogue. Both amorphous samples absorbed an order of magnitude less sodium than cesium, and the Hf-analogue absorbed more than twice the amount of sodium as the Zr analogue. The amorphous Hf-analogue exchanged 75% of its protons. The crystalline analogues exchange 2% (Zr) and 18% (Hf) of protons, without strong preference for Cs nor Na for the Zr analogue, and preference of Na over Cs for the Hf analogue. Notably, the crystalline HfP exchanged almost 10x more of its protons than the crystalline ZrP analogue. This result seems puzzling when compared to the studies summarized in **figure 8**, in which crystalline ZrP and HfP are similarly poor ion exchangers in these neutral conditions. However, different batches of crystalline ZrP and HfP were used for these

studies, and crystallinity may not be reproducible between batches. PXRD of the above described Cs/Na loaded samples provided further insight (**figure 9**). Consistent with compositional analysis, there is a greater shift in the crystalline HfP (002) peak at ~11.6° 2-theta and the peak at ~20° 2-theta, compared to the equivalent peaks for crystalline ZrP, upon ion-exchange. The shift to higher 2-theta represents a decrease in interlayer spacing with increasing Cs/Na intercalation. This may be due to accompanying decreased water in the interlayer space with increasing $H^+ \leftrightarrow A^+$ (A=alkali) exchange. Interestingly, we note that: (1) the peak widths for crystalline HfP are greater than those for crystalline ZrP and (2) peak widths for both analogues increase with ion exchange. This correlates with the increasing number of different phosphate environments observed by ^{31}P NMR, for the Cs-loaded samples.

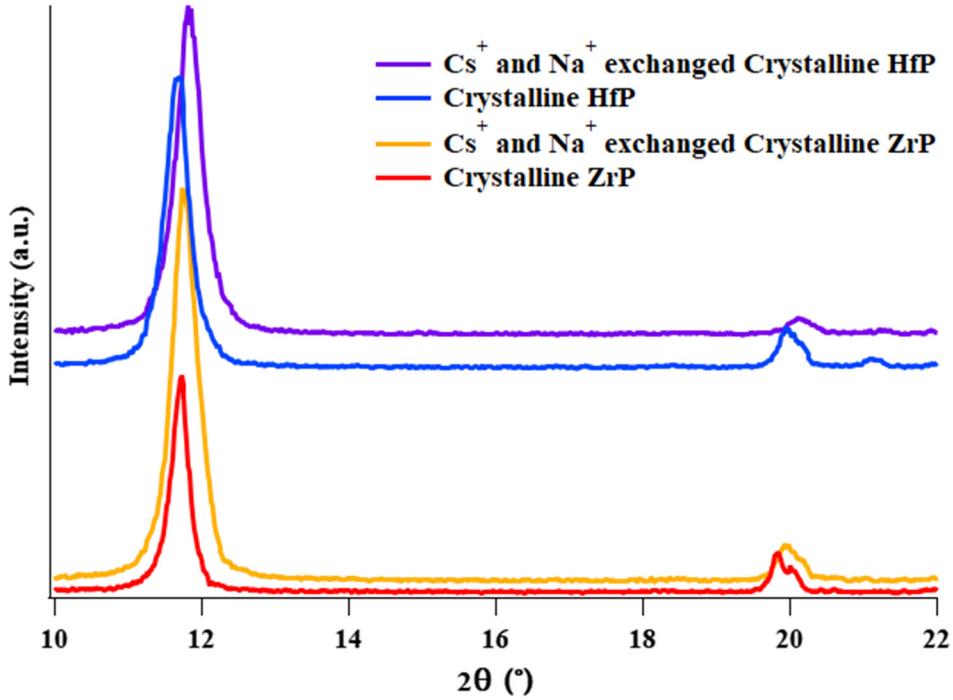

Figure 9. X-ray diffraction of crystalline HfP and ZrP, before and after cation-sorption from Na/Cs solutions.

In light of these results, we can conclude that under the same synthesis conditions, HfP exhibits lower crystallinity than ZrP, and this may be influenced by the relative solubility of the M-HPO_4 (M=Hf/Zr) ion pair in the aqueous synthesis media. During the hydrothermal process, there is continuous dissolution-precipitation of the material, and increased temperature and time of heating leads to more 'repairing' of disorder, ultimately leading to higher crystallinity. This process necessitates mobility of the lattice ions, which is accelerated by solubility. Notably, prior

optimized syntheses of crystalline materials utilized HF as a mineralizer, which increases the crystallinity, but as shown here, not necessarily the ion exchange function. Second, the more amorphous and disordered the ion-exchange phase, the better ion exchange behavior it exhibits (i.e. completeness of H^+-exchange). Certainly, comparing the Cs-loaded and Na/Cs-loaded crystalline analogues to amorphous analogues supports this conclusion (**Table 1**). At this point, we cannot accurately comment on the relative disorder (i.e. lack of crystallinity) of the amorphous HfP and ZrP. However, we do note (as stated prior) that amorphous ZrP exhibits a broad X-ray diffraction peak at <10° 2-theta, suggesting a poorly crystalline layered phase with higher interlayer spacing than crystalline α-Zr/HfP, and this peak is not observed for HfP (**figure 2**). The diffraction pattern of the amorphous ZrP looks most similar to a sample prepared at room temperature with a 25:1 H_3PO_4:$ZrOCl_2$ starting composition, recently reported by Zhou and colleagues.[33] They attributed the various degrees of poor crystallinity to turbostratic disorder.

The vast majority of prior studies of the ion-exchange behavior of Zr/HfP have been performed on ZrP, likely due to the cost and the assumption that Zr and Hf are essentially chemically identical. In this study we show that the amorphous or poorly crystalline analogues are more effective in removal of Cs from aqueous media, even in the presence of abundant Na. Moreover, a difference is noted between the crystalline analogues of HfP and ZrP—under identical synthesis conditions, the Hf-analogue exhibits poorer crystallinity, and this most likely translates to its observed superior ion exchange behavior.

Conclusions

From these preliminary comparative studies, we can conclude that ZrP will always exhibit higher order than HfP synthesized under identical conditions. This seems to be inherent to the respective Group IV metal cations, likely related to the poorer solubility of the Hf-PO_4 ion-pairs, compared to Zr-PO_4. This means during the synthesis process, with or without heating, more rapid precipitation of the HfP material will ensue. With more rapid precipitation and less crystal coarsening via Oswald-ripening-type crystal growth, HfP will always be more disordered than ZrP. Additionally, this family of materials demonstrates a clear correlation between poor order and ion exchange efficacy. This is directly related to surface area and high accessibility to interlayer space in the poorly ordered materials. In addition, abundant edge sites correlated with poor crystallinity may also contribute to the ion exchange capacities. This survey study brings to light the importance

of disorder in ion exchange behavior of the ZrP and HfP materials. Future studies we plan include structural analysis of the amorphous materials, optimizing synthesis to invoke poorer order in the Zr-analogues (since Zr is far more economical than Hf), and comparing the Sr-sorption behavior on the four Zr/HfP materials. Obvious paths to less crystalline materials include lower processing temperature (i.e. room temperature to 100 °C) or higher pH. Both options will be investigated to delineate materials characteristics in optimizing ion exchange capacity, selectivity, and kinetics, particularly toward separation of radioactive Sr and Cs for Na-rich solutions such as seawater.

Acknowledgements

CAN thanks the Summer Undergraduate Research Experience (SURE) of the College of Science, Oregon State University, for support to carry out this research that composed his Honor's Thesis. MN and KGB acknowledge support from Department of Energy, National Nuclear Security Administration, Award DE-NA0003763. Elemental analyses were performed in the WM Keck Collaboratory for Plasma Spectrometry housed within the College of Earth, Ocean and Atmospheric Sciences at Oregon State University. The solid state NMR experiments (TMA) were performed at Sandia National Laboratories which is a multi-mission laboratory managed and operated by National Technology & Engineering Solutions of Sandia, LLC, a wholly owned subsidiary of Honeywell International Inc., for the U.S. Department of Energy's National Nuclear Security Administration under Contract DE-NA0003525. This paper describes objective technical results and analysis. Any subjective views or opinions that might be expressed in the paper do not necessarily represent the views of the U.S. Department of Energy of the United States Government.

REFERENCES

(1) Miyamoto, N.; Yamamoto, S. Chapter 7 - Functional Layered Compounds for Nanoarchitectonics. In *Supra-Materials Nanoarchitectonics*; Ariga, K., Aono, M., Eds.; Micro and Nano Technologies; William Andrew Publishing, 2017; pp 173–192. https://doi.org/10.1016/B978-0-323-37829-1.00007-9.

(2) Uppuluri, R.; Gupta, A. S.; S. Rosas, A.; E. Mallouk, T. Soft Chemistry of Ion-Exchangeable Layered Metal Oxides. *Chemical Society Reviews* **2018**, *47* (7), 2401–2430. https://doi.org/10.1039/C7CS00290D.

(3) Sylvester, P.; Clearfield, A. The Removal of Strontium and Cesium from Simulated Hanford Groundwater Using Inorganic Ion Exchange Materials. *Solvent Extraction and Ion Exchange* **1998**, *16* (6), 1527–1539. https://doi.org/10.1080/07366299808934593.

(4) Liu, C.; Zachara, J. M.; Smith, S. C. A Cation Exchange Model to Describe Cs+ Sorption at High Ionic Strength in Subsurface Sediments at Hanford Site, USA. *Journal of Contaminant Hydrology* **2004**, *68* (3), 217–238. https://doi.org/10.1016/S0169-7722(03)00143-8.

(5) Fiskum, S. K.; Jr, D. L. B.; Arm, S. T.; Peterson, R. A. Cesium Removal from Simulated and Actual Hanford Tank Waste Using Ion Exchange. *Separation Science and Technology* **2005**, *40* (1–3), 51–67. https://doi.org/10.1081/SS-200041760.

(6) SYLVESTER, P.; BEHRENS, E. A.; GRAZIANO, G. M.; CLEARFIELD, A. An Assessment of Inorganic Ion-Exchange Materials for the Removal of Strontium from Simulated Hanford Tank Wastes. *Separation Science and Technology* **1999**, *34* (10), 1981–1992. https://doi.org/10.1081/SS-100100750.

(7) Silbernagel, R.; Shehee, T. C.; Martin, C. H.; Hobbs, D. T.; Clearfield, A. Zr/Sn(IV) Phosphonates as Radiolytically Stable Ion-Exchange Materials. *Chem. Mater.* **2016**, *28* (7), 2254–2259. https://doi.org/10.1021/acs.chemmater.6b00199.

(8) Osmanlioglu, A. E. Treatment of Radioactive Liquid Waste by Sorption on Natural Zeolite in Turkey. *Journal of Hazardous Materials* **2006**, *137* (1), 332–335. https://doi.org/10.1016/j.jhazmat.2006.02.013.

(9) Yıldız, B.; Erten, H. N.; Kış, M. The Sorption Behavior of Cs+ Ion on Clay Minerals and Zeolite in Radioactive Waste Management: Sorption Kinetics and Thermodynamics. *J Radioanal Nucl Chem* **2011**, *288* (2), 475–483. https://doi.org/10.1007/s10967-011-0990-5.

(10) Belousov, P.; Semenkova, A.; Egorova, T.; Romanchuk, A.; Zakusin, S.; Dorzhieva, O.; Tyupina, E.; Izosimova, Y.; Tolpeshta, I.; Chernov, M.; Krupskaya, V. Cesium Sorption and Desorption on Glauconite, Bentonite, Zeolite, and Diatomite. *Minerals* **2019**, *9* (10), 625. https://doi.org/10.3390/min9100625.

(11) Baek, W.; Ha, S.; Hong, S.; Kim, S.; Kim, Y. Cation Exchange of Cesium and Cation Selectivity of Natural Zeolites: Chabazite, Stilbite, and Heulandite. *Microporous and Mesoporous Materials* **2018**, *264*, 159–166. https://doi.org/10.1016/j.micromeso.2018.01.025.

(12) Rovira, A. M.; Fiskum, S. K.; Colburn, H. A.; Allred, J. R.; Smoot, M. R.; Peterson, R. A.; Colisi, K. M. Cesium Ion Exchange Testing Using Crystalline Silicotitanate with Hanford Tank Waste 241-AP-107. *Separation Science and Technology* **2019**, *54* (12), 1942–1951. https://doi.org/10.1080/01496395.2019.1577895.

(13) Celestian, A. J.; Kubicki, J. D.; Hanson, J.; Clearfield, A.; Parise, J. B. The Mechanism Responsible for Extraordinary Cs Ion Selectivity in Crystalline Silicotitanate. *J. Am. Chem. Soc.* **2008**, *130* (35), 11689–11694. https://doi.org/10.1021/ja801134a.

(14) Tripathi, A.; Medvedev, D. G.; Nyman, M.; Clearfield, A. Selectivity for Cs and Sr in Nb-Substituted Titanosilicate with Sitinakite Topology. *Journal of Solid State Chemistry* **2003**, *175* (1), 72–83. https://doi.org/10.1016/S0022-4596(03)00145-2.

(15) Nyman, M.; Hobbs, D. T. A Family of Peroxo-Titanate Materials Tailored for Optimal Strontium and Actinide Sorption. *Chem. Mater.* **2006**, *18* (26), 6425–6435. https://doi.org/10.1021/cm061797h.
(16) Nyman, M. D.; Hobbs, D. T. Hydrogen Peroxide Modified Sodium Titanates with Improved Sorption Capabilities. US7494640B1, February 24, 2009.
(17) Taylor-Pashow, K. M. L.; Missimer, D. M.; Jurgensen, A.; Hobbs, D. T. Characterization of Modified Monosodium Titanate – An Improved Sorbent for Strontium and Actinide Separations. *Separation Science and Technology* **2011**, *46* (7), 1087–1097. https://doi.org/10.1080/01496395.2011.554951.
(18) Duff, M. C.; Hunter, D. B.; Hobbs, D. T.; Fink, S. D.; Dai, Z.; Bradley, J. P. Mechanisms of Strontium and Uranium Removal from High-Level Radioactive Waste Simulant Solutions by the Sorbent Monosodium Titanate. *Environ. Sci. Technol.* **2004**, *38* (19), 5201–5207. https://doi.org/10.1021/es035415+.
(19) Dosch, R. G. *Application of Titanates, Niobates, and Tantalates to Neutralized Defense Waste Decontamination: Materials Properties, Physical Forms, and Regeneration Techniques. Final Report*; SAND-80-1212; Sandia National Labs., Albuquerque, NM (USA), 1981. https://doi.org/10.2172/6886911.
(20) Nyman, M.; Powers, C. R.; Bonhomme, F.; Alam, T. M.; Maginn, E. J.; Hobbs, D. T. Ion-Exchange Behavior of One-Dimensional Linked Dodecaniobate Keggin Ion Materials. *Chem. Mater.* **2008**, *20* (7), 2513–2521. https://doi.org/10.1021/cm800158u.
(21) Ding, N.; Kanatzidis, M. G. Permeable Layers with Large Windows in [(CH3CH2CH2)2NH2]5In5Sb6S19·1.45 H2O: High Ion-Exchange Capacity, Size Discrimination, and Selectivity for Cs Ions. *Chem. Mater.* **2007**, *19* (16), 3867–3869. https://doi.org/10.1021/cm071179g.
(22) Takahashi, A.; Tanaka, H.; Minami, K.; Noda, K.; Ishizaki, M.; Kurihara, M.; Ogawa, H.; Kawamoto, T. Unveiling Cs-Adsorption Mechanism of Prussian Blue Analogs: Cs+-Percolation via Vacancies to Complete Dehydrated State. *RSC Adv.* **2018**, *8* (61), 34808–34816. https://doi.org/10.1039/C8RA06377J.
(23) Seino, S.; Kawahara, R.; Ogasawara, Y.; Mizuno, N.; Uchida, S. Reduction-Induced Highly Selective Uptake of Cesium Ions by an Ionic Crystal Based on Silicododecamolybdate. *Angewandte Chemie* **2016**, *128* (12), 4055–4059. https://doi.org/10.1002/ange.201511633.
(24) Ding, D.; Zhang, Z.; Lei, Z.; Yang, Y.; Cai, T. Remediation of Radiocesium-Contaminated Liquid Waste, Soil, and Ash: A Mini Review since the Fukushima Daiichi Nuclear Power Plant Accident. *Environ Sci Pollut Res* **2016**, *23* (3), 2249–2263. https://doi.org/10.1007/s11356-015-5825-4.
(25) Mukai, H.; Hirose, A.; Motai, S.; Kikuchi, R.; Tanoi, K.; Nakanishi, T. M.; Yaita, T.; Kogure, T. Cesium Adsorption/Desorption Behavior of Clay Minerals Considering Actual Contamination Conditions in Fukushima. *Scientific Reports* **2016**, *6* (1), 21543. https://doi.org/10.1038/srep21543.
(26) Chen, G.-R.; Chang, Y.-R.; Liu, X.; Kawamoto, T.; Tanaka, H.; Parajuli, D.; Chen, M.-L.; Lo, Y.-K.; Lei, Z.; Lee, D.-J. Prussian Blue Non-Woven Filter for Cesium Removal from Drinking Water. *Separation and Purification Technology* **2015**, *153*, 37–42. https://doi.org/10.1016/j.seppur.2015.08.029.
(27) Lehto, J.; Koivula, R.; Leinonen, H.; Tusa, E.; Harjula, R. Removal of Radionuclides from Fukushima Daiichi Waste Effluents. *Separation & Purification Reviews* **2019**, *48* (2), 122–142. https://doi.org/10.1080/15422119.2018.1549567.
(28) Clearfield, A.; Stynes, J. A. The Preparation of Crystalline Zirconium Phosphate and Some Observations on Its Ion Exchange Behaviour. *Journal of Inorganic and Nuclear Chemistry* **1964**, *26* (1), 117–129. https://doi.org/10.1016/0022-1902(64)80238-4.

(29) Troup, J. M.; Clearfield, A. Mechanism of Ion Exchange in Zirconium Phosphates. 20. Refinement of the Crystal Structure of .Alpha.-Zirconium Phosphate. *Inorg. Chem.* **1977**, *16* (12), 3311–3314. https://doi.org/10.1021/ic50178a065.
(30) Sun, L.; J. Boo, W.; Sue, H.-J.; Clearfield, A. Preparation of α-Zirconium Phosphate Nanoplatelets with Wide Variations in Aspect Ratios. *New Journal of Chemistry* **2007**, *31* (1), 39–43. https://doi.org/10.1039/B604054C.
(31) Pica, M.; Donnadio, A.; Casciola, M. From Microcrystalline to Nanosized α-Zirconium Phosphate: Synthetic Approaches and Applications of an Old Material with a Bright Future. *Coordination Chemistry Reviews* **2018**, *374*, 218–235. https://doi.org/10.1016/j.ccr.2018.07.002.
(32) Ding, H.; Khan, S. T.; Aguirre, K. N.; Camarda, R. S.; Gafney, J. B.; Clearfield, A.; Sun, L. Exfoliation of α-Zirconium Phosphate Using Tetraalkylammonium Hydroxides. *Inorg. Chem.* **2020**, *59* (11), 7822–7829. https://doi.org/10.1021/acs.inorgchem.0c00937.
(33) Contreras-Ramirez, A.; Tao, S.; Day, G. S.; Bakhmutov, V. I.; Billinge, S. J. L.; Zhou, H.-C. Zirconium Phosphate: The Pathway from Turbostratic Disorder to Crystallinity. *Inorg. Chem.* **2019**, *58* (20), 14260–14274. https://doi.org/10.1021/acs.inorgchem.9b02442.
(34) Alberti, G.; Costantino, U.; Millini, R.; Perego, G.; Vivani, R. Preparation, Characterization, and Structure of α-Zirconium Hydrogen Phosphate Hemihydrate. *Journal of Solid State Chemistry* **1994**, *113* (2), 289–295. https://doi.org/10.1006/jssc.1994.1373.
(35) Clearfield, A.; Smith, G. D. Crystallography and Structure of .Alpha.-Zirconium Bis(Monohydrogen Orthophosphate) Monohydrate. *Inorg. Chem.* **1969**, *8* (3), 431–436. https://doi.org/10.1021/ic50073a005.
(36) Nakai, I.; Imai, K.; Kawashima, T.; Ohsumi, K.; Izumi, F.; Tomita, I. Synchrotron X-Ray Rietveld Analysis of α-Hafnium Phosphate. *Analytical Sciences* **1990**, *6* (5), 689–693. https://doi.org/10.2116/analsci.6.689.
(37) Salvadó, M. A.; Pertierra, P.; García-Granda, S.; García, J. R.; Rodríguez, J.; Fernández-Díaz, M. T. Neutron Powder Diffraction Study of α-Ti(HPO4)2.H2O and α-Hf(HPO4)2.H2O; H-Atom Positions. *Acta Cryst B* **1996**, *52* (5), 896–898. https://doi.org/10.1107/S0108768196006702.
(38) Clearfield, A.; Kalnins, J. M. On the Mechanism of Ion Exchange in Zirconium Phosphates—XIII: Exchange of Some Divalent Transition Metal Ions on α-Zirconium Phosphate. *Journal of Inorganic and Nuclear Chemistry* **1976**, *38* (4), 849–852. https://doi.org/10.1016/0022-1902(76)80369-7.
(39) Alberti, G.; Torracca, E. Crystalline Insoluble Salts of Polybasic Metals - II. Synthesis of Crystalline Zirconium or Titanium Phosphate by Direct Precipitation. *Journal of Inorganic and Nuclear Chemistry* **1968**, *30* (1), 317–318. https://doi.org/10.1016/0022-1902(68)80096-X.
(40) Dong, J.; Liu, L.; Li, J.; Li, Y.; Baerlocher, C.; McCusker, L. B. Synthesis, Characterization and Crystal Structure Analysis of an Open-Framework Zirconium Phosphate. *Microporous and Mesoporous Materials* **2007**, *104* (1), 185–191. https://doi.org/10.1016/j.micromeso.2007.02.003.
(41) Suárez, M.; Barcina, L. M.; Llavona, R.; Rodríguez, J. Layered Hafnium Phosphates. Synthesis, Characterization, Crystalline Structure and Intercalation Behaviour1Dedicated to Professor Abraham Clearfield for the Occasion of His 70th Birthday.1. *Journal of Molecular Structure* **1998**, *470* (1), 105–119. https://doi.org/10.1016/S0022-2860(98)00474-8.
(42) Tomita, I.; Aratake, K.; Saito, K.; Nakamura, T. Ion Exchange of Alkali Metals on Crystalline α-Hafnium Phosphate. *Analytical Sciences* **1987**, *3* (1), 35–40. https://doi.org/10.2116/analsci.3.35.
(43) Zamin, M.; Shaheen, T.; Dyer, A. Use of Amorphous Zirconium Phosphate for the Treatment of Radioactive Waste. *Journal of Radioanalytical and Nuclear Chemistry, Articles* **1994**, *182* (2), 345–348. https://doi.org/10.1007/BF02037510.
(44) Slobodyuk, A. B.; Didenko, N. A.; Godneva, M. M. An NMR Study of the Structure of Hydrated Fluorophosphatozirconates (Hafnates). *J Struct Chem* **2015**, *56* (6), 1063–1069. https://doi.org/10.1134/S0022476615060062.

(45) Maldonado-Manso, P.; Aranda, M. A. G.; Bruque, S.; Sanz, J.; Losilla, E. R. Nominal vs. Actual Stoichiometries in Al-Doped NASICONs: A Study of the Na1.4Al0.4M1.6(PO4)3 (M=Ge, Sn, Ti, Hf, Zr) Family. *Solid State Ionics* **2005**, *176* (17), 1613–1625. https://doi.org/10.1016/j.ssi.2005.04.009.

(46) Cheetham, A. K.; Clayden, N. J.; Dobson, C. M.; Jakeman, R. J. B. Correlations between 31P n.m.r. Chemical Shifts and Structural Parameters in Crystalline Inorganic Phosphates. *J. Chem. Soc., Chem. Commun.* **1986**, No. 3, 195–197. https://doi.org/10.1039/C39860000195.

(47) Martel, L.; Kovács, A.; Popa, K.; Bregiroux, D.; Charpentier, T. 31P MAS NMR and DFT Study of Crystalline Phosphate Matrices. *Solid State Nuclear Magnetic Resonance* **2020**, *105*, 101638. https://doi.org/10.1016/j.ssnmr.2019.101638.

(48) Nakayama, H.; Eguchi, T.; Nakamura, N.; Yamaguchi, S.; Danjyo, M.; Tsuhako, M. Structural Study of Phosphate Groups in Layered Metal Phosphates Byhigh-Resolution Solid-State31P NMR Spectroscopy. *J. Mater. Chem.* **1997**, *7* (6), 1063–1066. https://doi.org/10.1039/A607807I.

(49) Kong, X. Characterization of Proton Exchange Materials for Fuel Cells by Solid State Nuclear Magnetic Resonance. *Graduate Theses and Dissertations* **2010**. https://doi.org/10.31274/etd-180810-2893.

(50) MacLachlan, D. J.; Morgan, K. R. Phosphorus-31 Solid-State NMR Studies of the Structure of Amine-Intercalated .Alpha.-Zirconium Phosphate: Reaction of .Alpha.-Zirconium Phosphate with Excess Amine. *J. Phys. Chem.* **1990**, *94* (19), 7656–7661. https://doi.org/10.1021/j100382a062.

(51) Segawa, K.; Nakajima, Y.; Nakata, S.; Asaoka, S.; Takahashi, H. 31P-MASNMR Spectroscopic Studies with Zirconium Phosphate Catalysts. *Journal of Catalysis* **1986**, *101* (1), 81–89. https://doi.org/10.1016/0021-9517(86)90231-9.

(52) Chabé, J.; Bardet, M.; Gébel, G. NMR and X-Ray Diffraction Study of the Phases of Zirconium Phosphate Incorporated in a Composite Membrane Nafion®-ZrP. *Solid State Ionics* **2012**, *229*, 20–25. https://doi.org/10.1016/j.ssi.2012.10.006.

(53) Alberti, G. Syntheses, Crystalline Structure, and Ion-Exchange Properties of Insoluble Acid Salts of Tetravalent Metals and Their Salt Forms. *Acc. Chem. Res.* **1978**, *11* (4), 163–170. https://doi.org/10.1021/ar50124a007.

(54) Voronina, A. V.; Noskova, A. Y.; Semenishchev, V. S.; Gupta, D. K. Decontamination of Seawater from 137Cs and 90Sr Radionuclides Using Inorganic Sorbents. *Journal of Environmental Radioactivity* **2020**, *217*, 106210. https://doi.org/10.1016/j.jenvrad.2020.106210.

(55) Tomita, I.; Banju, M.; Noguchi, K.; Nakamura, T. Potassium-Ion Exchange on α-Hafnium Phosphate. *BCSJ* **1984**, *57* (11), 3281–3285. https://doi.org/10.1246/bcsj.57.3281.